EXPERIMENTAL INVESTIGATION ENERGY BALANCE AND DISTRIBUTION OF A TURBOCHARGED GDI ENGINE FUELLED WITH ETHANOL AND GASOLINE BLEND UNDER TRANSIENT AND STEADY-STATE OPERATING CONDITIONS

by

Xiongbo DUAN[a], Yiqun LIU[b], Xianjie ZHOU[a], Peng ZOU[a], and Jingping LIU[a*]

[a] State Key Laboratory of Advanced Design and Manufacturing for Vehicle Body, Hunan University, Changsha, China

[b] Department of Mechanical Engineering, Wayne State University, Detroit, Mich., USA

Original scientific paper
https://doi.org/10.2298/TSCI190112378D

In this paper, the energy balance and distribution of a turbocharged gasoline direc injection engine fuelled with ethanol and gasoline blend and powered the passenger car under transient and steady-state conditions were independently investigated. Then, the energy balance under transient conditions was comprehensively compared with steady-state behaviors under the bench test. The results indicated that the exhaust gas energy was much higher than the brake power at the high speed and high load zone. In addition, the maximum percentage of exhaust gas energy in total energy was located at high speed and medium load area, and showed a very good potential exhaust heat recovery. The coolant energy surpassed brake power and exhaust gas energy on the low speed and low load area and its percentage in total energy exceeded 30%, and in some operation points, it reached up to 50%. Compared energy balance under the transient condition with the steady-state condition, all the operating points were located on the low to medium speed and low to medium load area. In addition, the effective efficiency was located below the isolines of 25% or lower at the urban driving cycle, while the effective efficiency was much higher at extra urban driving cycle.

Key words: *energy balance, alternative fuel, transient condition, steady-state condition*

Introduction

Currently, energy conservation and emissions reduction have become an indispensable policy in the whole world [1]. It is obvious that the automotive sector consumes a large number of traditional fossil fuels by the gasoline and Diesel engines. Meanwhile, as one of the most widely used power machine, internal combustion engine (ICE) emit a huge amount of harmful pollution emissions [2], such as, CO, HC, and NO_x. Emission regulations and fuel consumption regulations of ICE have been increasingly stringent to drive the ICE to enhance fuel conversion efficiency and reduce emissions in recent years [3]. Consequently, it is essential to conduct some fundamental experiments coupled with advanced control strategies (multi-injection and EGR, *etc.*) and alternative fuels (alcohols, ethers and hydrogen, and so on) on

* Corresponding author, e-mail: liujp2018@gmail.com

the whole map of the ICE, in order to understand the energy flow and energy distributions for improving the fuel conversion efficiency and reducing exhaust emissions.

Fuel conversion efficiency is one of the most key evaluation factors involved with the ICE [4-6]. In order to enhance the fuel conversion efficiency or effective thermal efficiency, researchers have already conducted heat balance or energy balance on ICE for understanding the distribution of energy based on the First law of thermodynamics [7, 8]. Thus, it is of most significant to evaluate the fraction of each term where losses occur in engines. As a matter of fact, fuel energy which is supplied to the ICE could be cursorily divided into three parts on certain conditions: energy converted into effective work, energy transferred into coolant water, and energy dissipated into exhaust gas [9, 10]. However, the proportion of each term in the ICE strongly depends on the operating conditions. Gharehghani *et al.* [11] investigated thermal balance on a turbocharged spark-ignition engine fuelled with natural gas, and showed that the percentage of transferred energy to exhaust gases increased by increasing engine load and coolant temperature. Payri *et al.* [3] carried the experimental analysis of the global energy balance on a direct injection Diesel engine, and concluded that the variation of the coolant temperature had an almost negligible effect in terms of efficiency while cooling the air yields in an improvement about 1% and advancing the start of injection about 1.5%. Abedin *et al.* [12] reviewed the energy balance of ICE using alternative fuels, which discussed the basic energy balance theory in details along with the variations in energy balance approaches and terms. Martin *et al.* [13] investigated thermal analysis on a light-duty compression ignition engine operating with diesel-gasoline dual-fuel combustion mode, results showed that increasing the low reactivity fuel leads to a better shape of the heat release rate, with a reduction of heat transfer and exhaust losses, thus improving the thermal efficiency about 1% with respect to a conventional diesel combustion. However, the aforementioned energy balance and exergy analysis on engines were compared under steady-state operating conditions. In other words, the test engines were operated at fixed speed and load for a while until the values of temperature sensors, pressure sensors and flow meters almost kept the same level. Thus, according the first law of thermodynamics [14], it is easy to calculate the energy that transferred to coolant water, exhaust gas and converted into useful work.

On the other hand, the passenger vehicle powered by the ICE always operated under transient conditions, such as acceleration and deceleration. Therefore, there exists a huge difference of ICE between actual behaviors under vehicle driving conditions and steady-state performance under the bench test [5], namely, the energy or heat balance intimately relies on the transient performance of the ICE. In order to investigate the gap of the energy balance of the ICE between transient and steady-state operating conditions, researchers also have conducted many experiments on this issue. Razmara *et al.* [15] used an optimal control method based on exergy which was introduced for transient and steady-state operation of ICE, and results showed that using the exergy-based optimal control strategy resulted in an average of 6.7% fuel saving and 8.3% exergy saving compared to commonly used the first law of thermodynamics. Rakopoulos *et al.* [16] developed a computer model for studying the First- and Second-law (availability) balances of a turbocharged Diesel engine under transient load conditions, and revealed that, at least for the specific engine type and operation, a thermodynamic, dynamic or design parameter can have a conflicting impact on the engine transient response as regards energy and availability properties. Singh *et al.* [17] analyzed in detail the various energy losses at different engine operating regimes and quantified of losses and understood of loss mechanism serve as a starting point for future technologies to recover the lost energy. Others researcher conducted experiments on the engines for energy recovery from the exhaust gas [18, 19] and coolant water [20, 21] to reduce the time of warm up.

In this study, the energy balance and distribution of a turbocharged direct injection gasoline engine were experimentally investigated and the variation of output brake work, transferred energy to the coolant water and exhaust gas energy under transient conditions of vehicle driving on new European driving cycle (NEDC) and steady-state of the bench test were comprehensively compared. First, some necessarily technical adaptations were conducted on the engine and the passenger car in order to install test rigs, measuring systems and data logger system, and accurately measure and collect data. Second, the energy balance and change rules of each term were investigated on the gasoline direct injection (GDI) engine which powered the passenger vehicle and operated under the transient conditions of NEDC. Then, the GDI engine was carefully removed from the passenger car and installed on the test bench. Furthermore, some test rigs, measuring systems and data logger system were installed on the GDI engine. Last but not least, the energy balance was conducted on the engine which operated on steady-state by sweeping the speed and load. Eventually, energy balance and distribution were compared and analyzed based on the mapping characteristic and NEDC that it was disassembled into urban driving cycle (UDC) and extra urban driving cycle (EUDC).

Experimental apparatus and procedures

Transient experiment on the chassis dynamometer

In this test, the energy balance test was conducted on a passenger car under the chassis dynamometer in a climatic chamber, and the schematic diagram of the test facilities layout is shown in fig. 1. The specifications of the turbocharged GDI (TGDI) engine are listed in tab. 1. Meanwhile, the specifications of the tested passenger car are given in tab. 2. The passenger car was fastened on the chassis dynamometer in order to simulate the reality road conditions. All subsystems were controlled by the main control system.

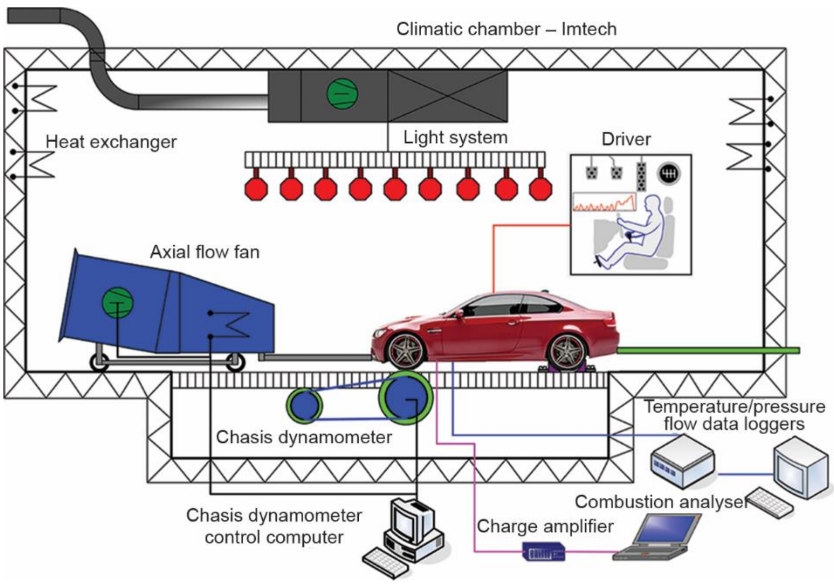

Figure 1. Schematic diagram of test facilities for the passenger car

Table 1. The specifications of TGDI engine

Item	Content
ICE type	In-line four cylinder, four-stroke
Bore, [mm]	76
Stroke, [mm]	82.6
Compression ratio, [–]	10
Number of valves per cylinder	4
Displacement, [L]	1.5
Connecting rod length, [mm]	133.2
Respiration	Turbocharged
Injection mode	Gasoline direction injection

Table 2. The specifications of tested vehicle

Item	Content
Mass, [kg]	1365
Frontal area, [m^2]	2.250
Coefficient of aerodynamic drag, [–]	0.298
Rolling radius, [m]	0.316
Transmission ratios, [–]	4.044, 2.371, 1.556, 1.159, 0.852, 0.672
Final drive ration, [–]	3.685
Maximum speed, [kmh^{-1}]	160
Drive type	Front engine front wheel drive

To ensure collected data have a good accuracy, the range and precisions of various instruments, including sensors, flow meters, were carefully selected and accurately calibrated, tab. 3. To be more specific, in-cylinder pressure was measured by the Kistler piezoelectric sensor. The platinum resistance thermometer (Pt100) sensors were used to measure the temperature of air intake and coolant water, while the K-type thermometer was utilized to test the temperature of exhaust gas. The mass-flow rate of air intake was measured through Sensiflow, and the mass-flow rate of coolant water was measured by the Tokyo Keiso Electromagnetic Flow Meter, whilst the transient fuel consumption of ICE was tested through the AVL fuel mass-flow meter. Meanwhile, the passenger car was placed in the thermostatic chamber for 24 hours at 25 °C to maintain the same temperature of each part or assembly of the passenger car. Then, energy balance test on the passenger car was conducted on the chassis dynamometer.

Stead-state experiment on the test bench

After the passenger car was conducted on energy balance test on the chassis dynamometer. Then, the GDI engine was carefully removed from the passenger car and installed on the test bench. Specifically, the GDI engine shaft was coupled to an AVL electronic dynamometer, which was utilized to absorb the load and control the speed of test engine. Figure 2 is a schematic illustration of the test rigs, equipment, sensors and flow meters in steady-state energy balance test. Then, the GDI engine was conducted the energy balance experiment on the test bench under steady-state conditions in the laboratory.

It is noted that the thermal hysteresis exists in the energy accumulation and time lags behind during the data collection. Admittedly, it is difficult to eliminate this error and becomes a major error source during the transient experiment under the NEDC. In addition, the data acquisition system used the filter functions to eliminate the disturbance of the extreme data. Specifically, the overall experimental uncertainty was 2.76%, and this value met the engineering requirements within the limitation 5%. Therefore, the results met the accuracy requirements on engineering practice. Furthermore, in this paper, we qualitatively analyzed and compared the energy balance and energy distribution on the turbocharged GDI engine. Through the whole research of this paper, the characteristics and influence factors of energy balance of ICE under transient conditions (NEDC) of vehicle driving and steady-state of the bench test were depicted in detail. Meanwhile, some suggestions were proposed to enhance the actual fuel conversion efficiency of ICE and recover the energy from the exhaust gas and coolant water.

Results and discussions

Comparative analysis of the total energy

This paper aimed at to evaluate the energy balance and distribution on a TGDI engine which operated under the transient and steady-state conditions. Subsequently, the energy balance and its fraction were investigated by comparison and analysis based on the mapping characteristic and NEDC. Figures 3 and 4 present the fuel mass-flow rate and the total energy of the passenger car which was operated under NEDC of cold starting on the cha-

Table 3. The specifications of main test instruments

Instrument	Calibrated range	Accuracy
Torque sensor (home-made)	0-500 Nm	±1%
In-cylinder pressure (piezoelectric sensor Kistler 6055BB)	0-150 bar	0.9% FS
Amplifier (Kistler 5015)	–10-10 V	0.01 V
Fuel consumption meter (AVL fuel mass-flow meter 735S)	0-125 kg/h	±0.12%
Wind-speed sensor (Keiso RF-1000)	0-50 m/s	±1%
Air flow meter (Sensiflow DN80)	0-720 kg/h	±1%
Coolant mass-flow (Keiso electromagnetic flowmeters)	0-350 L/min	±0.5%
Exhaust gas temperature sensor (K-type thermocouple)	0-1000 °C	±1.5 °C
Air intake temperature (Pt100)	0-200 °C	±0.2 °C
Coolant water temperature (Pt100)	0-200 °C	±0.2 °C
Pressure sensor (piezo-resistive transducers)	0-6 bar	0.1% FS

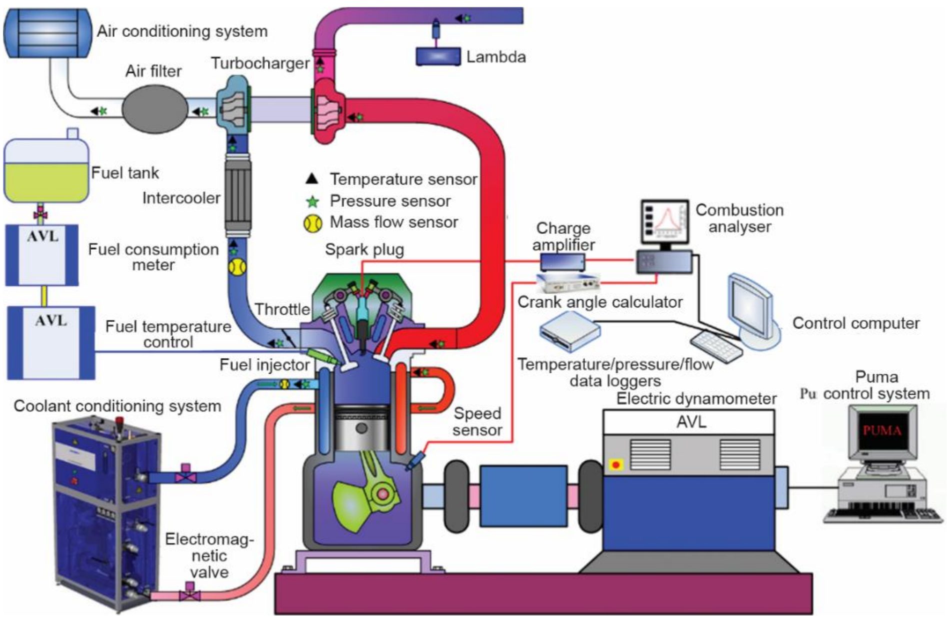

Figure 2. Schematic of the test rigs and equipment layout of engine under steady-state test

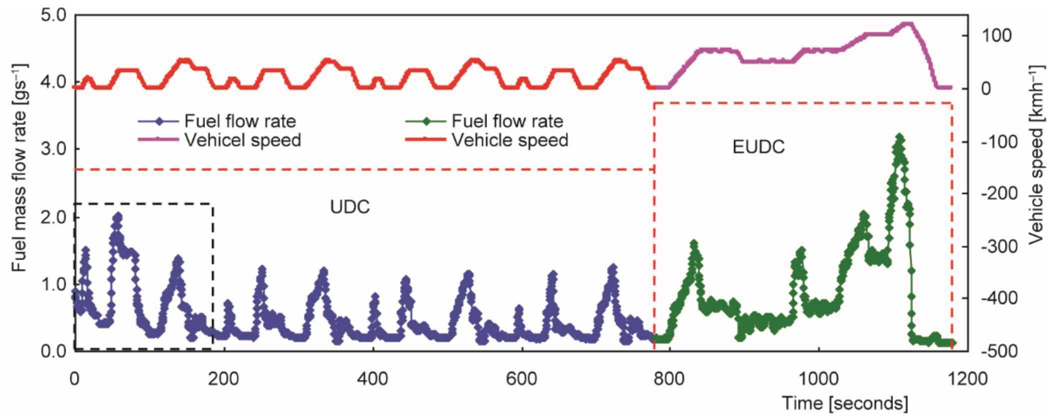

Figure 3. The mass-flow fuel rate of the passenger car operated on transient conditions

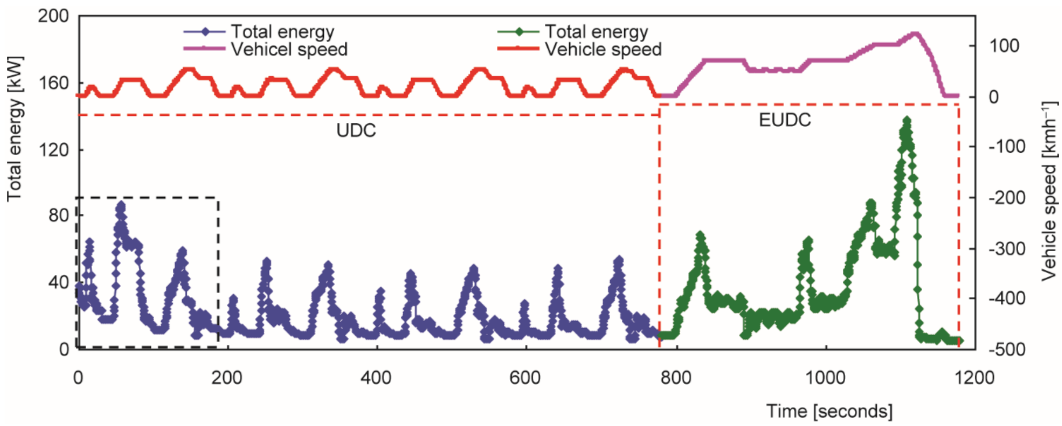

Figure 4. The total energy of the passenger car operated on transient conditions

sis dynamometer, respectively. Sincethe engine was operated on the transient conditions, the speed and load of the engine can be changed dramatically in real-time. As one can see, when the passenger car was operated on the EUDC, the fuel mass-flow rate was much higher than the UDC. This is due to the fact that when the passenger car was operated on the EUDC, the engine consumed much more fuel for operating on the higher speed and higher load.

Figures 5(a) and 5(b) display the mass-flow rate of fuel and the total energy of the engine under steady-state operating conditions by mapping characteristic, respectively. As illustrated in fig. 5(a), the mass-flow rate of the fuel moderately increased with increasing the speed and load, so did the total energy, as shown in fig. 5(b). When the GDI engine was tested on the bench, the temperature of the output coolant water was approximately 85 °C. At the same time, the temperature and mass-flow rate of the output coolant water was automatically controlled by AVL553. From fig. 5, when the engine operated on the high speed and high load area, the engine consumed a large amount of fuel, and thereby releasing a huge of energy. However, in the real road operating conditions, the GDI engine, which powered the passenger car, rarely operated on these conditions. Almost all the operating conditions were located in the low to medium speed and low to medium and high load.

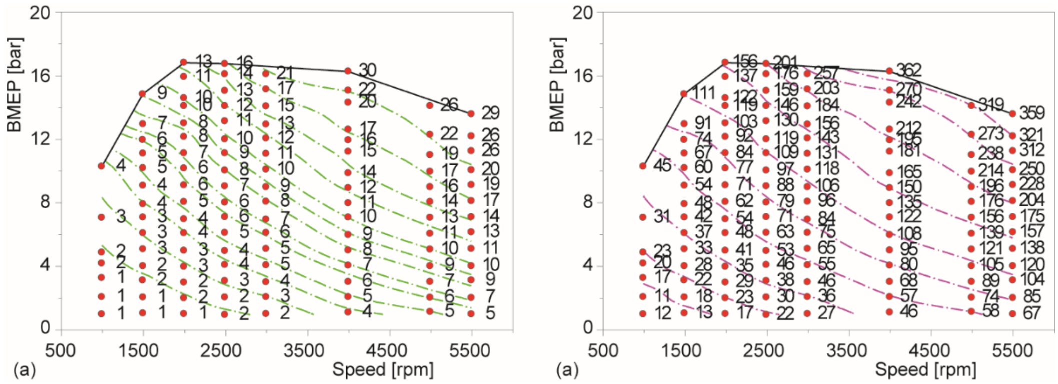

Figure 5. The mass-flow rate of fuel and total energy of the engine operated on steady-state conditions; (a) the mass-flow rate of fuel [kgh^{-1}], (b) the total energy [kW]

Figures 6(a) and 6(b) compare the mass-flow rate of fuel and total energy when the GDI engine powered the passenger car and operated on under transient conditions (NEDC) and steady-state conditions by mapping characteristics, respectively. Green dots represent EUDC operating points and black dots represent EUDC operating points. Every operating point is regarded as a quasi-static thermodynamic equilibrium. It can be seen from fig. 6, when the passenger car operated the NEDC on the chassis dynamometer, all the operating points were located in the low speed area of the map. The speed of engine was less than 2600 rpm. However, the load strongly depended on the engine operating conditions. When the passenger car was operated on EUDC, the mass-flow rate of fuel was much high, which released a huge of energy in the cylinder to meet requirement of the high power.

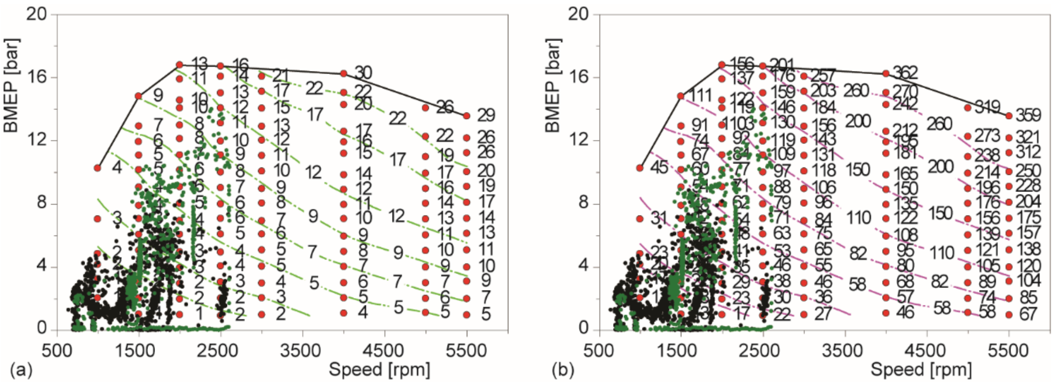

Figure 6. Comparison of the fuel mass-flow rate and total energy of the engine operated on transient and steady-state conditions; (a) the mass-flow rate of fuel [kgh^{-1}], (b) the total energy [kW]

Comparative analysis of effective work distribution

Figures 7 and 8 demonstrate the effective power and the effective efficiency of the passenger car which was operated under NEDC on the chassis dynamometer, respectively. It can be seen that the change rule of the effective power was the same as with the fuel mass-flow rate. Since FMEP initial value was large due to the low temperature of the coolant and oil in the first 200 seconds (as illustrated in the black dashed bordered rectangle). Therefore, the effective efficiency was lower in the first 200 seconds than the rest of the time of the NEDC. Moreover, when the passenger car was operated on the EUDC, the effective power was much high since the GDI engine was operated on the high speed and medium and high load area.

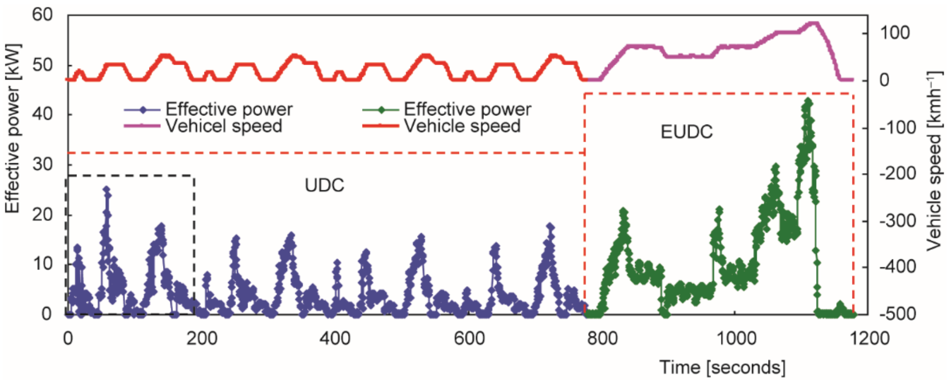

Figure 7. The effective power of the passenger car operated on transient condition

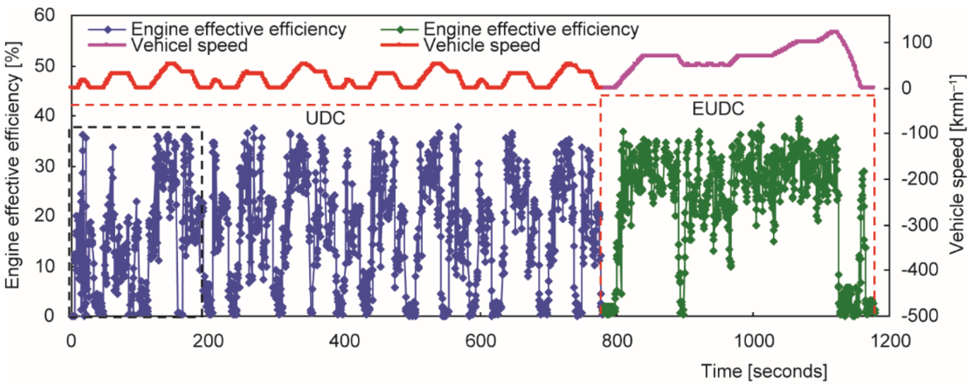

Figure 8. The effective efficiency of the passenger car operated on transient conditions

Figures 9(a) and 9(b) illustrate the brake power and effective efficiency of the GDI engine operated on steady-state conditions by mapping characteristics, respectively. In maps, the independent variables are speed and load (BMEP), whilst the dependent variables are the brake power and effective efficiency. From fig. 9(a), it was observed that the brake power increased with increasing speed and load (as depicted in blue dashed circle marked region). When the engine operated on the high speed and high load area, the brake power was much higher than the low speed and load (as shown in black dashed circle marked region). Meanwhile, the air/fuel ratio was enriched in these operation conditions. However, the effective efficiency was reached peak at medium speed and medium load are, as demonstrated in fig. 9(b) in the black dashed circle marked region. Importantly, effective efficiency directly determines the brake specific fuel consumption (BSFC) of the ICE. Furthermore, it ultimately determines the fuel conversion efficiency and fuel economy of the ICE.

Figures 10(a) and 10(b) compare the brake power and effective efficiency of the GDI engine operated under transient and steady-state conditions by mapping characteristics, respectively. It is very easy to find that when the passenger car operated on the transient con-

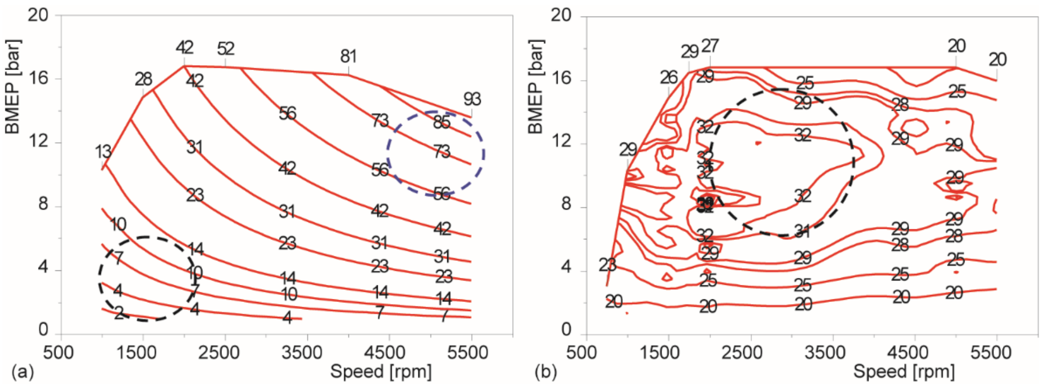

Figure 9. The brake power and effective efficiency of the engine operated on steady-state conditions; (a) the brake power [kW], (b) the effective efficiency [%]

ditions, almost all the operating points were located in the low to medium speed and low to medium load. Specifically, when the passenger car operated on the UDC conditions, the effective efficiency was located below the isolines of 25% or lower. More seriously, the effective efficiency even approached to 0% in some cases due to idle. When the passenger car operated on the EUDC conditions, the effective efficiency was much higher than that UDC conditions, as shown in blue dashed circle marked region. Most of the operating points were located in the maximum efficiency zone (except sharp deceleration points at the end of the NEDC). Thus, it was highly suggested that the ICE should operate on the medium speed and medium load. The chemical energy of the fuel releases in-cylinder by the combustion process and converted into brake power through heat-work conversion. Under the same of fuel mass-flow rate, the more brake power is converted, the higher effective efficiency can be obtained. Therefore, enhancing effective efficiency is a determining factor to improve the fuel conversion efficiency.

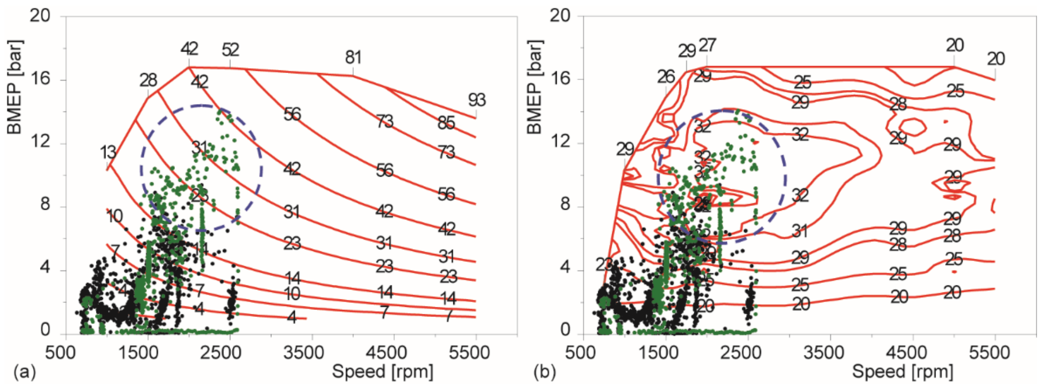

Figure 10. Comparison of the brake power and efficiency of the engine operated on transient and steady-state conditions; (a) the brake power [kW], (b) the effective efficiency [%]

Comparative analysis of exhaust gas energy distribution

Figures 11 and 12 depict the exhaust gas energy and the percentage of exhaust gas energy in total energy of the passenger car which was operated under NEDC on the chassis dynamometer, respectively. From fig. 13, the exhaust gas energy was slightly higher than the effective power in the first 200 seconds of the NEDC (as illustrated in the black dashed bordered rectangle) and in the end of EUDC (as shown in the red dashed bordered rectangle). It indicates that the chemical energy of fuel was wasted into the ambient. On the other hand, the temperature of the coolant and oil were lower in the first 200 seconds of the NEDC. If the exhaust gas energy was recovered and reused to heat the intake air and cold ICE during the low temperature season (winter, high-latitude area) and initial start ICE, the engine could warm faster and reduce fuel consumption.

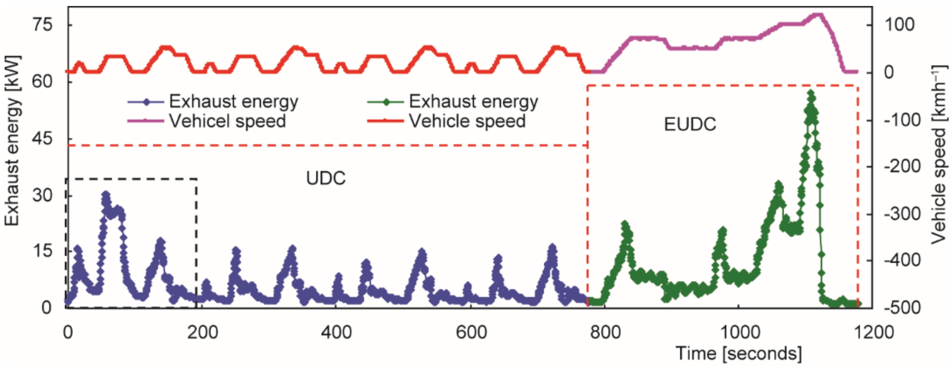

Figure 11. The exhaust gas energy of the passenger car operated on transient condition

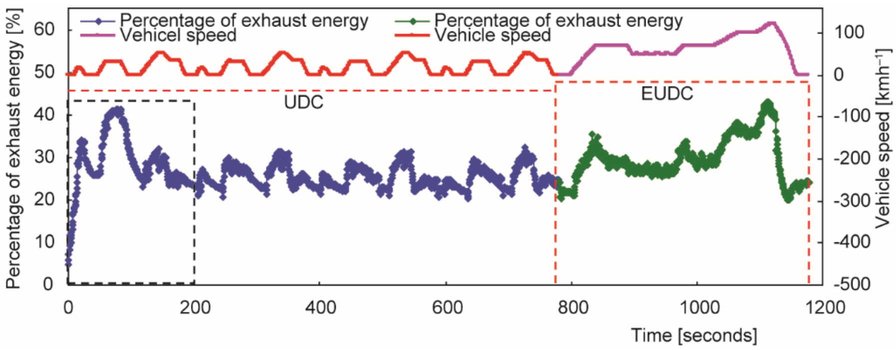

Figure 12. The percentage of the exhaust gas energy in total energy on transient conditions

Figures 13(a) and 13(b) reveal the exhaust gas energy and the percentage of exhaust gas energy in total energy of the GDI engine operated under steady-state conditions by mapping characteristics, respectively. As one can see, when the GDI engine was operated on the low speed and low load area (as shown in the black dashed circle region), the exhaust gas energy was approximately equivalent to the brake power compared with fig. 9(a). However, the exhaust gas energy was much higher than the brake power at the high speed and high load area (as illustrated in the blue dashed circle zone). Furthermore, the maximum percentage of exhaust gas energy in total energy was located in high speed and medium load while the maximum percentage of the effective efficiency in total energy was located in medium speed and medium load area. This phenomenon can be explained as follows: when the GDI engine was operated on the high speed and high load area, the fuel mixture was enriched to decrease the in-cylinder temperature and avoid knocking and abnormal ignition. Subsequently, the energy of unburned fuel was stored in the remainder heat loss. Therefore, the percentage of the exhaust gas in total energy declined and located in medium speed and medium load. On the other hand, the FMEP dramatically increased with increasing speed and load [22], when the engine was operated in the high speed and high load area, both the friction loss and the mass-flow rate of fuel were also increased. Thus, the maximum percentage of the effective efficiency in total energy was located in medium speed and medium load.

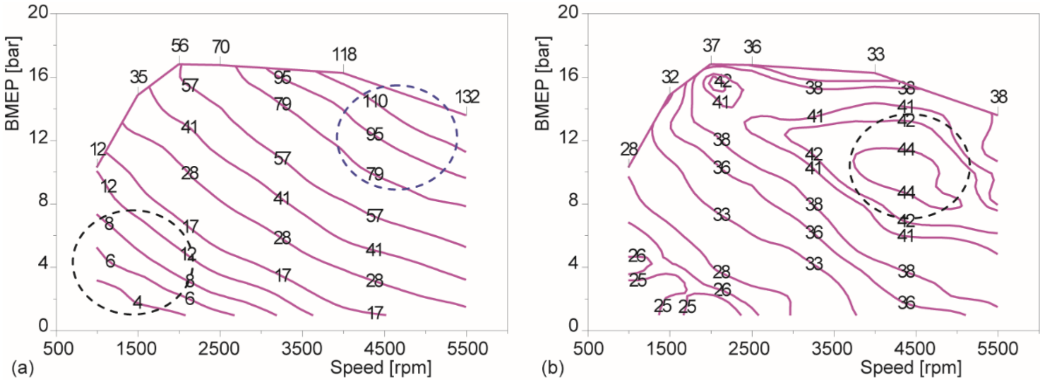

Figure 13. The exhaust gas energy and its percentage in total energy of the engine operated on steady-state conditions; (a) the exhaust gas energy [kW], (b) percentage of exhaust gas energy in total energy [%]

Figures 14(a) and 14(b) compare the exhaust gas energy and the percentage of the exhaust gas in total energy of the GDI engine operated under transient and steady-state conditions by mapping characteristics, respectively. It is observed that almost all the operation points were located at the low load (as shown in the black dashed rectangle marked area) when the passenger car was operated on the UDC. As described earlier, the exhaust gas energy was approximately equivalent to the brake power compared with fig. 9(a). To be more specific, the exhaust gas energy located between 4 kW and 14 kW, so did the brake power. Moreover, the percentage of the exhaust gas energy in total energy was located between 25% and 30%, so did the effective efficiency. It indicates that exhaust gas energy contained huge of energy and showed highly potential heat recovery. Furthermore, when the engine was operated on the EUDC, many operating points were located in the high load (as shown in the red

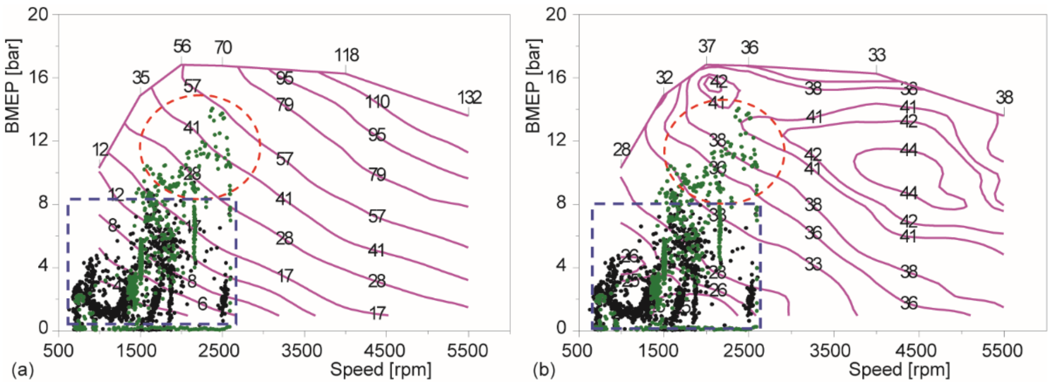

Figure 14. Comparison of exhaust gas energy and its percentage in total energy under transient and steady-state conditions; (a) the exhaust gas energy [kW], (b) percentage of exhaust gas energy in total energy [%]

dashed circle marked area), and the exhaust gas energy surpassed the brake power compared with fig. 5(a). Meanwhile, the percentage of the exhaust gas energy in total energy exceeded 40%. Thus, if the exhaust gas energy could be recovered and reused, the fuel conversion efficiency and the effective efficiency of the ICE will be dramatically enhanced [23].

Comparative analysis of coolant energy distribution

Figures 15 and 16 show the coolant energy and the percentage of coolant energy in total energy of the passenger car which was operated under NEDC on the chassis dynamometer, respectively. Since the passenger car was cold started and the initial coolant temperature was at 25 °C, the coolant energy increased from zero at the beginning of the NEDC. When the passenger car was operated on the UDC, the coolant energy fluctuated in a certain range. Under idling operating conditions, the coolant energy reached its lowest value. In general, the coolant energy was less sensitive to the passenger car operating conditions compared with effective power and exhaust gas energy. This is due to the fact that heat transfer was much slower than other forms of energy. However, things were changed in coolant energy in total energy, particularly under the sudden change acceleration and deceleration operating conditions. The sudden acceleration and deceleration were caused biggish fluctuations of the percentage coolant energy in total energy. This is because the sharp acceleration and deceleration led to rapidly increasing and decreasing fuel mass-flow rate, see fig. 4, and then the total

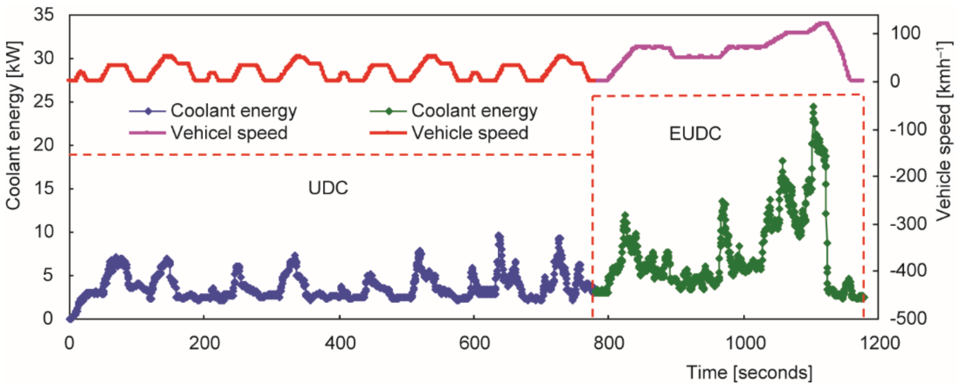

Figure 15. The coolant energy of the passenger car operated on transient conditions

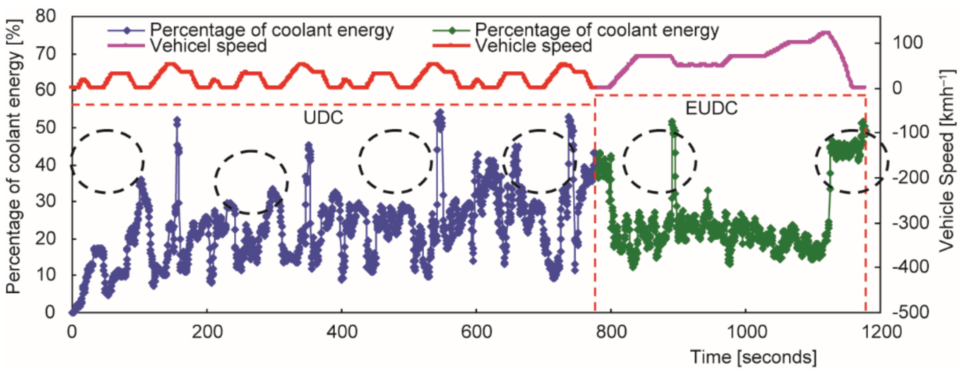

Figure 16. The percentage of the coolant energy in total energy on transient conditions

energy was significantly changed whilst the coolant energy changed slowly. Therefore, it caused the peaks of the percentage of coolant energy.

Figures 17(a) and 17(b) depict the coolant energy and the percentage of coolant energy in total energy of the GDI engine operated under steady-state conditions by mapping characteristics, respectively. The coolant energy surpassed brake power and exhaust gas energy compared fig. 9(a) and fig. 13(a) when the GDI engine was operated on the low speed and low load area (as shown in the red dashed circle region). Moreover, the percentage of coolant energy in total energy exceeded 30%, and in some operating points, it reached up to 50% (as shown in the red dashed circle region). This is due to the fact that the output brake power was small and most of the fuel energy was changed into friction work and heat transfer loss and both of them were transferred to the coolant finally. However, when the engine was operated on the high speed and high load area (as shown in the black dashed circle region), things was changed in coolant energy and its percentage in total energy. The coolant energy increased, but the magnitude of the fuel mass-flow rate significantly increased, resulting in the total fuel energy dramatically increased. Thus, the percentage of the coolant energy in total energy decreased. In general, if the coolant energy is recovered and reused, the fuel conversion efficiency and the effective efficiency of the ICE will be improved.

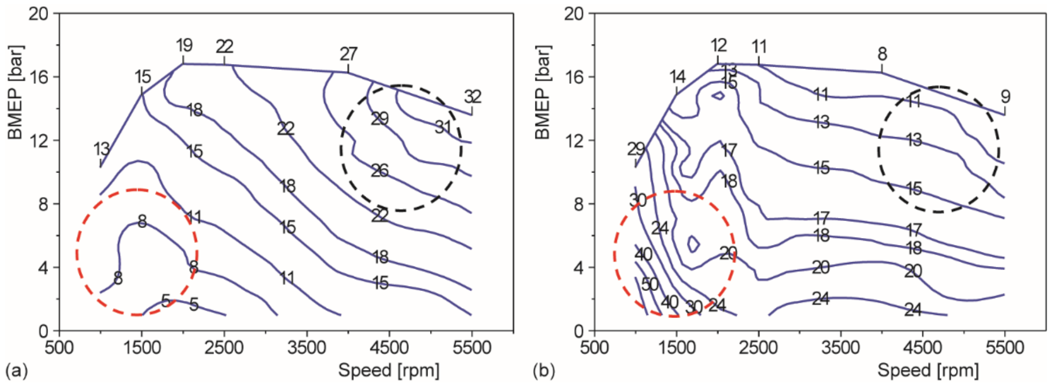

Figure 17. The coolant energy and its percentage in total energy of the engine operated on steady-state conditions; (a) the coolant energy [kW], (b) the percentage of coolant energy in total energy [%]

Figures 18(a) and 18(b) compare the coolant energy and its percentage in total energy of the GDI engine under transient and steady-state conditions by mapping characteristics, respectively. It is observed that almost all the operating points were located in the low speed and low load area, and the percentage of coolant energy in total energy surpassed 30% when the passenger car was operated on the UDC. However, when the passenger car was operated on the EUDC, some operating points were located in the medium load zone. Compared fig. 9(b) and fig. 13(b), although the coolant energy increased with the load, the percentage of the coolant energy in total energy decreased due to the total fuel energy increase greatly. Thus, it is highly suggested that the passenger car (the engine) should operate at the high load for better fuel conversion efficiency and the effective efficiency.

Finally, since the remainder heat loss is dissipated in the ambient by heat radiation and convection, and could not be recovered or reused. Therefore, it is not discussed here. It is noted that the algorithm method was used to interpolate transient sampling data in each time step (interval time step: 1 second). Then, calculating each energy term individually and its

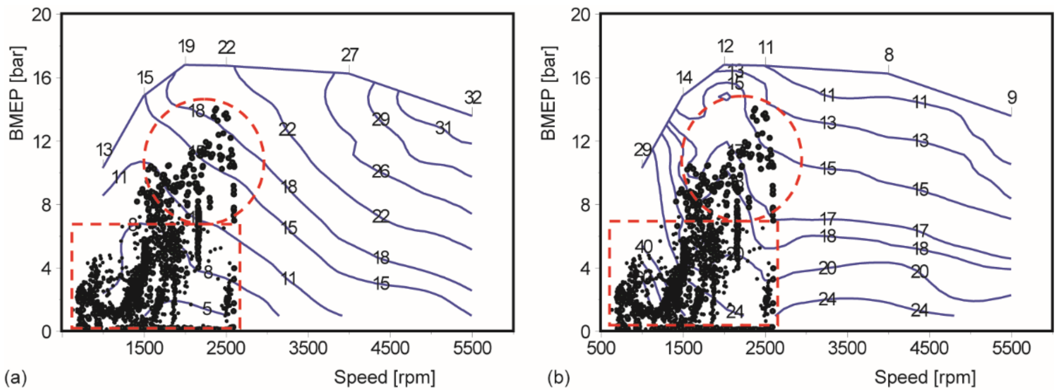

Figure 18. Comparison of the coolant energy and its percentage of the engine operated on transient and steady-state conditions; (a) the coolant energy [kW], (b) the percentage of coolant energy in total energy [%]

percentage in the total energy. Eventually, mapping each transient energy term and its ratio in the steady plotted data, respectively.

Conclusions

In this study, the energy balance and distribution of a TGDI engine fuel with ethanol and gasoline blend and powered the passenger car under transient and steady-state conditions were independently investigated. Then, the energy balance under transient conditions was comprehensively compared with steady-state condition behaviors under the bench test. Finally, the differences of energy balance between transient and steady-state conditions were comparatively analyzed and the influencing factors were revealed. The main conclusions are summarized as follows.

- Exhaust gas energy was much higher than the brake power at the high speed and high load zone, and showed a very good potential exhaust heat recovery. The coolant energy surpassed brake power and exhaust gas energy on the low speed and low load area and its percentage in total energy exceeded 30%, and in some operation points, it reached up to 50%.
- Under transient condition, all operating points were located on the low to medium speed and low to medium load area. Moreover, the speed of the GDI engine was less than 2600 rpm, and its load strongly depended on the operating conditions. In addition, the effective efficiency were located below the isolines of 25% or lower at the UDC, while the effective efficiency was much higher at EUDC.

Acknowledgment

This research work is sponsored by the National Natural Science Foundation of China (NO. 51776061). The first author appreciates the China Scholarship Council (File No. 201706130033) and Hunan University for supporting as a visiting scholar. The authors appreciate the anonymous reviewers and the editor for careful reading and many constructive comments and suggestions to enhance the manuscript.

References

[1] Guo, G., *et al.,* Visual Experimental Investigations of String Cavitation and Residual Bubbles in the Diesel Nozzle and Effects on Initial Spray Structures, *International Journal of Engine Research*, On-line first, https://doi.org/10.1177/1468087418791061, 2018

[2] Duan, X., *et al.,* Performance, Combustion and Knock Assessment of a High Compression Ratio and Lean-Burn Heavy-Duty Spark-Ignition Engine Fuelled with N-Butane and Liquefied Methane Gas Blend, *Energy, 158* (2018), Sept., pp. 256-268
[3] Payri, F., *et al.,* Experimental Analysis of the Global Energy Balance in a DI Diesel Engine, *Applied Thermal Engineering, 89* (2015), Oct., pp. 545-557
[4] Li, T. T., *et al.,* Energy Distributions in a Diesel Engine Using Low Heat Rejection (LHR) Concepts, *Energy Conversion Management, 130* (2016), Dec., pp. 14-24
[5] Duan, X., *et al.,* Influence of Single Injection and Two-Stagnation Injection Strategy on Thermodynamic Process and Performance of a Turbocharged Direct-Injection Spark-Ignition Engine Fuelled with Ethanol and Gasoline Blend, *Applied Energy, 228* (2018), Oct., pp. 942-953
[6] Duan, X., *et al.* Experimental and Numerical Investigation of the Effects of Low-Pressure, High-Pressure and Internal EGR Configurations on the Performance, Combustion and Emission Characteristics in a Hydrogen-Enriched Heavy-Duty Lean-Burn Natural Gas SI Engine, *Energy Conversion and Management, 195* (2019), Sept., pp. 1319-1333
[7] Payri, F., *et al.,* Experimental and Theoretical Analysis of the Energy Balance in a DI Diesel Engine, SAE technical paper, 2015-01-1651, 2015
[8] Romero, C., *et al.,* Energy Balance During the Warm-up of a Diesel Engine, SAE technical paper, 2014-01-0676, 2014
[9] Taymaz, I., An Experimental Study of Energy Balance in Low Heat Rejection Diesel Engine, *Energy, 31* (2006), 2-3, pp. 364-371
[10] Zheng, J., *et al.,* Second Law Analysis of a Low Temperature Combustion Diesel Engine: Effect of Injection Timing and Exhaust Gas Recirculation, *Energy, 38* (2012), 1, pp. 78-84
[11] Gharehghani, A., *et al.,* Experimental Investigation of Thermal Balance of a Turbocharged SI Engine Operating on Natural Gas, *Applied Thermal Engineering, 60* (2013), 1-2, pp. 200-207
[12] Abedin, M. J., *et al.,* Energy Balance of Internal Combustion Engines Using Alternative Fuels, *Renewable Sustainable Energy Reviews, 26* (2013), Oct., pp. 20-33
[13] Martín, J., *et al.,* Thermal Analysis of a Light-Duty CI Engine Operating with Diesel-Gasoline Dual-Fuel Combustion Mode, *Energy, 115* (2016), Nov., pp. 1305-1319
[14] Heywood, J. B., *Internal Combustion Engine Fundamentals*, McGraw-hill, Inc., New York, USA, 1988
[15] Razmara M., *et al.* Optimal Exergy-Based Control of Internal Combustion Engines, *Applied Energy, 183* (2016), Dec., pp. 1389-1403
[16] Rakopoulss, C., *et al.,* Comparative First- and Second-Law Parametric Study of Transient Diesel Engine Operation, *Energy, 31* (2006), 12, pp. 1927-1942
[17] Singh, S., *et al.,* Analysis of Thermal Balance of Diesel Engine and Identification of Scope for Waste Heat Recovery, SAE technical paper 2013-01-2744, 2013
[18] Nwosu, P. N., *et al.,* Thermal Modeling of a Novel Thermosyphonic Waste Heat Absorption System for Internal Combustion Engines, *Energy, 71* (2014), July, pp. 21-31
[19] Shon, J., *et al.,* Improved Heat Storage Rate for an Automobile Coolant Waste Heat Recovery System Using Phase-Change Material in a Fin-Tube Heat Exchanger, *Applied Energy, 113* (2014), Jan., pp. 680-689
[20] Hamdy, M., *et al.,* An Overview on Adsorption Cooling Systems Powered by Waste Heat from Internal Combustion Engine, *Renewable Sustainable Energy Reviews, 51* (2015), Nov., pp. 1223-1234
[21] Wu, Z., *et al.,* A High Efficiency Oxyfuel Internal Combustion Engine Cycle with Water Direct Injection for Waste Heat Recovery, *Energy, 70* (2014), June, pp. 110-120
[22] Rahmani, R., *et al.,* The Effect of Cylinder Liner Operating Temperature on Frictional Loss and Engine Emissions in Piston Ring Conjunction, *Applied Energy, 191* (2017), Apr., pp. 568-581
[23] Duan, X., *et al.*, Experimental Study on the Energy Flow of a Gasoline-Powered Vehicle under the NEDC of Cold Starting, *Applied Thermal Engineering, 115* (2017), Mar., pp. 1173-1186

Paper submitted: January 12, 2019
Paper revised: August 27, 2019
Paper accepted: September 12, 2019